Synthesis and Oxygen Reduction Reaction Activity of Atomic and Nanoparticle Gold on Thiol-Functionalized Multiwall Carbon Nanotubes

Electrochemical and Solid-State Letters, **14** (10) B105-B109 (2011)
1099-0062/2011/14(10)/B105/5/$28.00 © The Electrochemical Society

Synthesis and Oxygen Reduction Reaction Activity of Atomic and Nanoparticle Gold on Thiol-Functionalized Multiwall Carbon Nanotubes

Junhyung Kim, Seung Woo Lee, Shuo Chen, and Yang Shao-Horn*,z

Electrochemical Energy Laboratory and Department of Mechanical Engineering, Massachusetts Institute of Technology, Cambridge, Massachusetts 02139, USA

We demonstrated the self-assembly of atomic Au on thiol-functionalized multiwall carbon nanotubes through covalent bonding and the formation of Au nanoparticles (NPs) upon a subsequent thermal treatment. Au NPs of 3.4 nm were found to exhibit higher ORR activity than that of 1.9 nm, which can be attributed to removal of thiols from Au NP surfaces. This hypothesis is supported by decreasing intrinsic ORR activity with increasing alkanethiol-coverage on polycrystalline-Au. The understanding on top of the novel synthetic route has led to the development of Au NPs less than 5 nm with the highest ORR activity reported to date.
 [DOI: 10.1149/1.3612270]

Manuscript submitted April 25, 2011; revised manuscript received June 27, 2011. Published July 20, 2011.

Organic-layer-protected Au colloids with controlled particle sizes and shapes have been studied extensively due to their novel electronic and optical properties.[1,2] Recently Au nanoparticles (NPs) have been explored for electro-oxidation of small organic molecules[3–6] and oxygen reduction reaction (ORR).[7–9] Of particular interest is to examine how the electrochemical activity of Au NPs changes with their particle size.[3,10] Although the optical properties and electrochemical capacitance of alkanethiol-monolayer-protected Au NPs obtained from colloid methods have been well studied as a function of their particle sizes,[11] it is not straightforward to determine the intrinsic electrocatalytic activity of Au NPs as a function of size because the type and coverage of surfactants[10,12] and surface atomic structure[13–15] on the Au NPs can greatly influence the activity. For example, McFarland et al.[10] have shown that the intrinsic ORR activity (Au-surface-area-normalized current density) of Au NPs dispersed on high-surface-area support increases with decreasing particle size from 7 to 3 nm. On the other hand, Sun et al.[12] have reported the mass-normalized ORR currents of Au NPs of 3, 6 and 8 nm, having the highest for 8 nm and the lowest for 6 nm, where the intrinsic ORR activity (true-surface-area normalized currents) of Au NPs has not been reported. This ambiguity may come from the fact that active surface sites of Au NPs of different synthetic routes can be blocked by dissimilar surfactants such as block co-polymers,[10] oleylamines[12] and thiols[12] to different degrees. Here we focus on the synthesis of Au in the range from a few atoms to ~3 nm on thiol-functionalized multiwall carbon nanotubes (MWNTs), and examine how the thiol functional groups affect the ORR kinetics on the Au surfaces.

In this letter, we develop novel self-assembly of a few atoms of Au on thiol-functionalized multiwall carbon nanotubes (HS-MWNTs) through covalent bonding.[15] We show that Au NP size can be controlled in the range from 1.9 ± 0.4 to 3.4 ± 0.5 nm by a subsequent heat-treatment (Fig. 1a). ORR activity of Au NPs/MWNTs in 0.1 M KOH by using a rotating disk electrode (RDE) technique showed that the 3.4 nm Au NPs/MWNTs have higher intrinsic and mass ORR activity than those of atomic Au and 1.9 nm Au NPs/MWNTs. This ORR activity difference can be attributed to removal of thiols on the Au NP surfaces with increasing annealing temperature, which is further supported by additional ORR measurements of polycrystalline Au disks modified with different C_6S coverage.

Experimental

For thiol-functionalized multiwall carbon nanotubes (HS-MWNTs), commercially available MWNTs (NANOLAB, 95% purity, length 1–5 μm, outer diameter 15 ± 5 nm) were stirred in concentrated H_2SO_4/HNO_3 (3:1, v:v), for 2 h to prepare carboxylic acid functionalized MWNTs (COOH-MWNTs), and then chlorinated by refluxing for 12 h with $SOCl_2$ at 70°C. After evaporating any remaining $SOCl_2$, HS-MWNTs were subsequently obtained by reaction with $NH_2(CH_2)_2SH$ in dehydrated toluene for 24 h at 70°C. The HS-MWNT powder was dried under vacuum at 60°C overnight.

Direct deposition of Au atoms on HS-MWNTs was obtained from the following processes. 10 ml aqueous $HAuCl_4$ (6.9 mg) was added into a suspension of 20 mg of the thiol-functionalized MWNTs in 32 ml Milli-Q water, equivalent to 20 wt % ratio of Au to MWNTs. Sonication of the suspension for 15 min, which was followed by vigorous stirring in an ice bath for another 15 min, led to self-assembly of Au onto the thiol-functionalized MWNTs (AuP-S-MWNTs). The AuP-S-MWNT sample was then washed thoroughly in Milli-Q water to remove soluble unattached Au^{3+} precursors. AuP-S-MWNTs were re-dispersed in Milli-Q water by sonication and were reduced by rapid addition of 2 ml of $NaBH_4$ (7.6 mg) at 5°C, and then were stirred subsequently for 1 h. Immediately following the reduction, the powder was washed with Milli-Q water and ethanol, and was filtered several times using a nylon membrane filter, and then was dried in air at 25°C for 12 h (Au-S-MWNTs). Finally, annealing Au-S-MWNTs at 300, 400, or 500°C in a mixture of 4% H_2 and 96% Ar (volume %) for 1 h in an Image furnace (ULVAC-RIKO, MILA-5000, ULVAC Technologies, Inc.) led to the formation of spherical-like Au NPs of different sizes.

X-ray photoelectron spectroscopy (XPS) analysis was used to probe the valence state of gold species at AuP-S-MWNTs and Au-S-MWNTS using a Kratos AXIS Ultra Imaging X-ray photoelectron spectrometer. All spectra were calibrated with the C 1s photoemission peak for sp^2 hybridized carbons at 284.5 eV. Curve fitting of the photoemission spectra was done after a Shirley type background subtraction.

A Jeol 2010F transmission electron microscope (TEM) was applied to examine the particle size. Equipped with a field emission electron gun and operated at 200 kV, the point-to-point resolution of this TEM is 0.19 nm. To study the beam irradiation effect on Au precursor on MWNTs, the TEM was set at 250 K magnification with electron beam current density of 68 pA/cm^2, which was measured by the fluorescent screen inside the TEM. During imaging process, the electron beam intensity was below 30 pA/cm^2 and it took less than 2 min to adjust the focus and take the image.

Direct current plasma-atomic emission spectroscopy (DCP-AES) was used to analyze the weight loading of Au NPs on the MWNTs using a Beckman spectra Span VI DCP-AES instrument. The Au NPs/MWNTs samples were dissolved in concentrated aqua regia and then diluted for analysis. Calibration curves were made from dissolved standards with concentrations from 0 to 100 ppm in the same acid matrix as the unknowns.

* Electrochemical Society Active Member
z E-mail: shaohorn@mit.edu

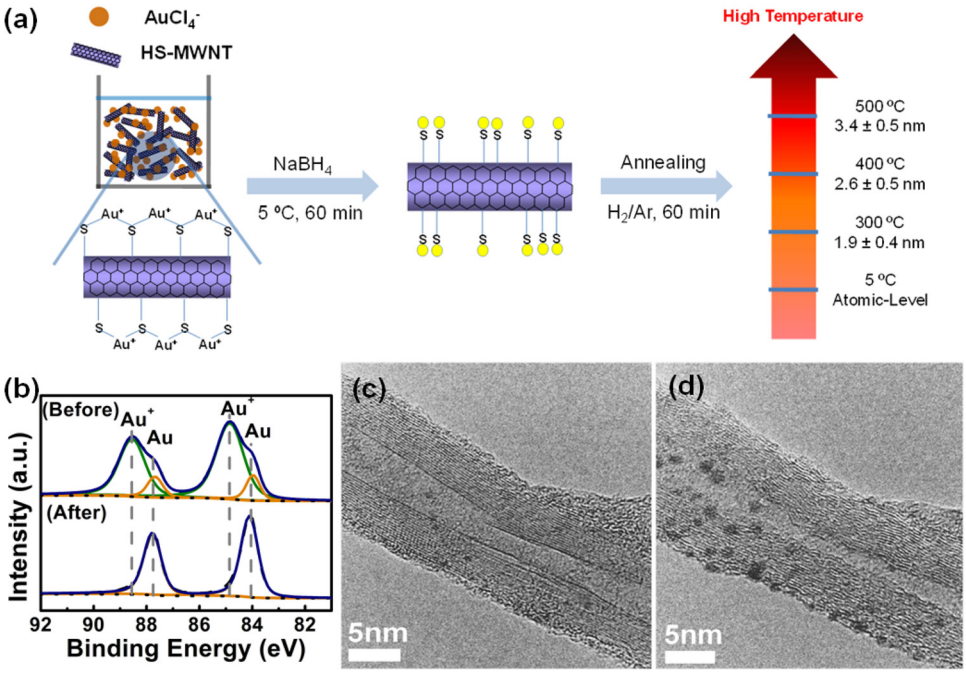

Figure 1. (Color online) (a) Schematic of self-assembly of Au atoms onto the thiol-functionalized MWNT surfaces and growth of Au NPs on the MWNTs at different annealing temperatures, (b) XPS **spectra** of Au 4f for Au-S-MWNTs before and after reduction by $NaBH_4$, TEM images of Au-S-MWNT taken (c) immediately and (d) after 15 min TEM electron-beam irradiation.

For Au NPs/MWNTs electrode preparation, 20 μL dispersed solution of Au NPs/MWNTs in Milli-Q water and ethanol mixture (3:1, volume ratio) was applied onto a glassy carbon disk electrode (0.196 cm^2 geometrical surface area) substrate. After evaporating the solvent, the deposited Au NPs/MWNTs thin film was covered with 10 μL of 0.05 wt % Nafion® solution to attach the Au NPs/MWNTs to the glassy carbon disk. The electrode was then dried under air atmosphere with a cover glass and transferred to the electrochemical cell in Ar-saturated 0.1 M KOH electrolyte.

The electrochemical measurements were carried out in a three-electrode cell using a saturated calomel electrode (SCE) as the reference and a platinum wire as the counter electrode using a voltamaster potentiostat (Radiometer analytical, France). Potentials in the text are referred to the reversible hydrogen electrode (RHE) scale, calibrated via the hydrogen oxidation/reduction reaction on a pure Pt rotating disk electrode (RDE) in the same cell and electrolyte at the same temperature. Cyclic voltammetry was conducted at a scan rate of 20 mV/s in Ar-saturated 0.1 M KOH electrolyte and Electrochemical surface area (ESA) of Au was determined from the charge associated with oxide reduction of Au electrode (240 $\mu C/cm^2_{Au}$) after double layer correction in the cathodic scan potential at ~1.1 V vs. RHE.[16] ORR was measured in O_2 saturated 0.1 M KOH at 10 mV/s scan rate after bubbling O_2 for 25 min. In the RDE experiments, the working electrode was rotated in the range of 100–2500 rpm using a PINE Instruments AFMSRCE rotator. Analysis of the kinetic current was determined from RDE measurements using Koutecky-Levich equation.[17,18]

Results and Discussion

The direct deposited Au atom on thiol-functionalized MWNTs as described in experimental section was probed by X-ray photoelectron spectroscopy (XPS) analysis and Transmission electron microscopy (TEM). XPS of Au 4f collected from AuP-S-MWNT showed Au^+ ($4f_{7/2}$ 88.5 eV) but not Au^{3+} ($4f_{7/2}$ 89.8 eV) as a dominant species,[19] suggesting the formation of covalent bonds between Au^+ species and the thiol-functional groups on MWNTs (**Fig.** 1b). Furthermore, only Au^0 was observed after reduction and no Au^+

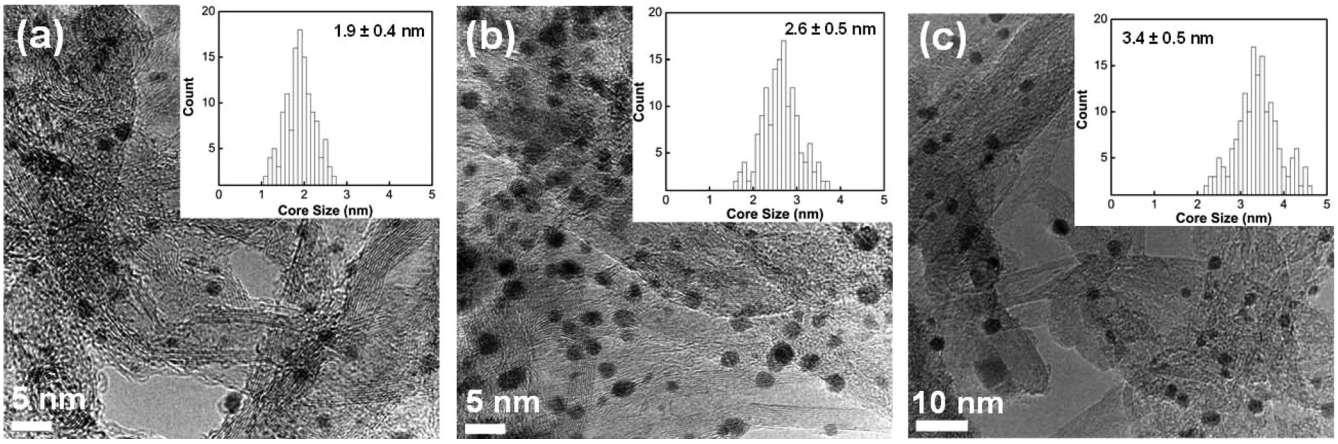

Figure 2. TEM images of heat-treated Au NPs/MWNTs at (a) 300°C, (b) 400°C and (c) 500°C. The particle size histogram with its mean diameter and standard deviation collected from ~150 particles for each sample is shown in the Figure inset.

species was detected (Fig. 1b), which confirms full reduction of Au precursors to Au atoms on MWNTs. TEM imaging (Fig. 1c) of Au-S-MWNTs initially showed no visible Au nanoclusters. Interestingly, Au NPs were found to gradually appear under TEM electron beam irradiation after 15 min with an accelerating voltage of 200 kV, leading to coalescence of Au atoms and the formation of ~1.5 nm Au NPs (Fig. 1d).

It should be noted that low-temperature reduction is the key to prepare atomic Au on the thiol-functionalized MWNTs. Au-S-MWNTs prepared by reduction at room temperature lead to large (>10 nm) and non-uniform particles. This is in contrast to the synthesis of Pt NPs on the MWNTs reported previously,[20] where Pt atoms on the thiol-functionalized MWNTs could be obtained from H_2PtCl_6 by $NaBH_4$ reduction at room temperature. Although the details of Au and Pt NP formation mechanisms have not been completely dissected, the difference might be attributed to higher mobility of Au than that of Pt atoms at room temperature.

Annealing Au-S-MWNTs in a mixture of 4% H_2 and 96% Ar (volume %) in an Image furnace (ULVAC-RIKO, MILA-5000, ULVAC Technologies, Inc.) led to the formation of spherical-like Au NPs of different sizes. Figure 2 shows the temperature dependence of Au NP sizes, having 1.9 ± 0.4 nm at 300°C with 15.0 wt % ratio of Au atom to MWNT, 2.6 ± 0.5 nm at 400°C (18.1 wt %) and 3.4 ± 0.5 nm at 500°C (17.7 wt %). The temperature-dependent Au NP sizes can be explained according to Shi's thermodynamical model,[21] where Au NPs with lower melting points grow until they become stable at a specific annealing temperature. It is in contrast to multistep synthetic methods reported previously,[22,23] where size control becomes difficult and agglomeration of Au NPs occurs with increasing annealing temperature.

Electrochemically active surface area (ESA) of Au was investigated from cyclic voltammetry (Fig. 3a). Only capacitive currents were found for Au-S-MWNTs. On the other hand, Au NPs/MWNTs of 1.9 and 3.4 nm were found to exhibit electrochemical oxidation and reduction of Au in the cyclic voltammograms (CVs) (Fig. 3a). The Au ESA of Au NPs/MWNTs was obtained from the charge associated with reduction of Au oxides (corresponding to the reduction peak at 1.1 V vs. RHE).[24] Although Au particle sizes were found to grow (Fig. 2), the ESA of Au NPs/MWNTs was found to increase with increasing annealing temperature, as shown in Fig. 3a. This observation can be explained by the removal of thiols from Au NP surfaces upon annealing, leading to smaller thiol coverage on Au NPs (leading to more electrochemically active surface Au) of larger sizes obtained at higher temperatures.

We further examined the ORR activity of Au NPs/MWNTs in 0.1 M KOH by using a rotating disk electrode (RDE) technique (details in experimental section). Au NPs/MWNTs of 1.9 and 3.4 nm were found more active for ORR than MWNTs (HS-MWNTs) in O_2-saturated 0.1 M KOH, where the onset potential of ORR current of Au NPs/MWNTs of 3.4 nm was found to shift positively relative to Au NPs/MWNTs of 1.9 nm, as shown in Fig. 3b. Considering that Au loading of Au NPs/MWNTs of 1.9 nm was considerably higher than that of 3.4 nm on glassy carbon, the positive shift in the ORR onset potential in Fig. 3b indicates higher mass ORR activity for Au NPs of 3.4 nm, which can be attributed largely to lower thiol coverage on surface Au upon annealing at 500°C. This is supported by the following observations: (1) the disappearance of Au redox peaks in the CV of hexanethiol-passivated Au NPs/MWNTs (C_6S-Au-NPs/MWNTs) by introducing hexanethiol ($CH_3(CH_2)_4CH_2SH$, C_6S) into the dispersion of Au NPs/MWNTs of 3.4 nm (Fig. 3a); (2) the hexanthiol coverage of Au NPs of 3.4 nm led to a large negative shift in the ORR onset potential (Fig. 3b). It should be mentioned that heat-treatment can remove thiol groups as well as change surface atomic structure of Au NPs, both of which can influence ORR activity. For example, previous studies have shown that the (100) surface of Au is significantly more active than the (111) and (110) surfaces.[25] As TEM imaging showed that Au NPs remained nearly spherical during heating from 1.9 to 3.4 nm, the enhanced ORR activity from 1.9 to 3.4 nm can be attributed primarily to thiol removal from Au NPs. However, some additional contributions from increasing (100) surfaces of Au NPs from 1.9 to 3.4 nm to the enhanced ORR activity cannot be excluded. Interestingly, mass-normalized ORR currents of Au NPs/MWNTs of 3.4

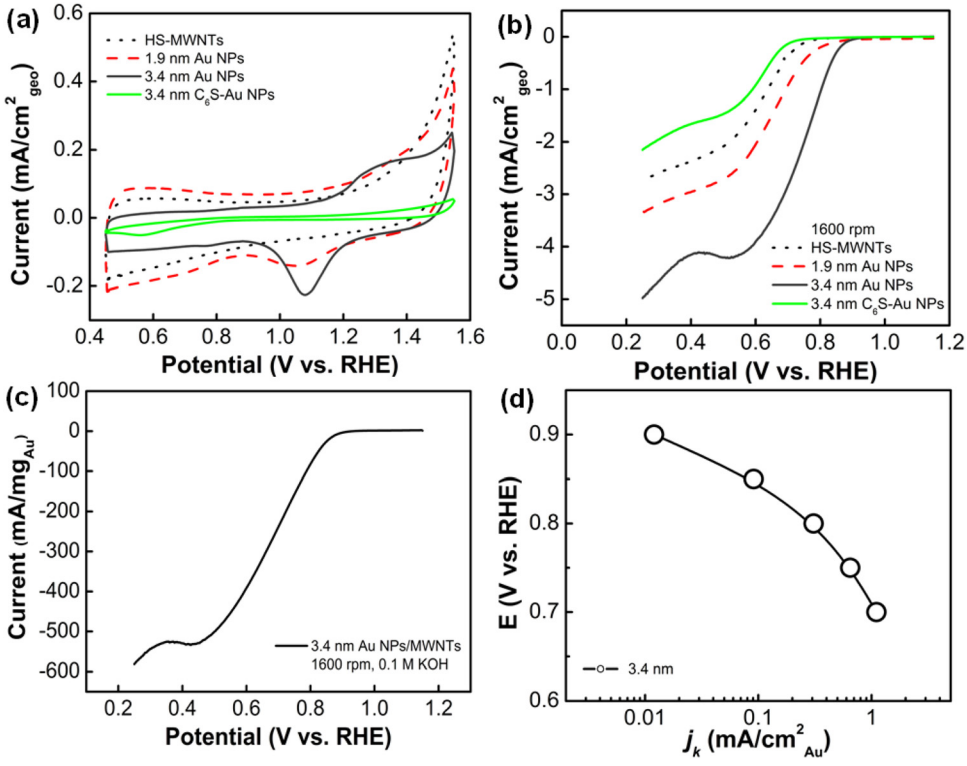

Figure 3. (Color online) (a) Cyclic voltammograms of Au NPs/MWNTs on glassy carbon electrode (GCE) in Ar-saturated 0.1 M KOH at a scan rate of 20 mV/s, where 1.9 nm Au NPs/MWNTs, 3.4 nm Au NPs/MWNTs and C_6S-3.4 nm Au NPs/MWNTs electrodes have a loading of 23.5, 7.1, and 7.1 $\mu g_{Au}/cm^2_{geo}$, respectively. (b) background-corrected RDE polarization curve of Au NPs/MWNTs and C_6S-Au NPs/MWNTS on GCE in O_2-saturated 0.1 M KOH collected at 1600 rpm and a scan rate of 10 mV/s, where ORR currents were subtracted by background current in Ar and normalized by the RDE geometry area, (c) I-V curve of 3.4 nm Au NPs/MWNTs catalysts in oxygen saturated 0.1 M KOH as a function of potential at a rotation speed of 1600 rpm and a scan rate of 10 mV/s. Oxygen reduction current was normalized by mass of Au NPs and (d) kinetic current density of 3.4 nm Au NPs/MWNTs in O_2 reduction reaction at 1600 rpm from Koutecky-Levich analysis.

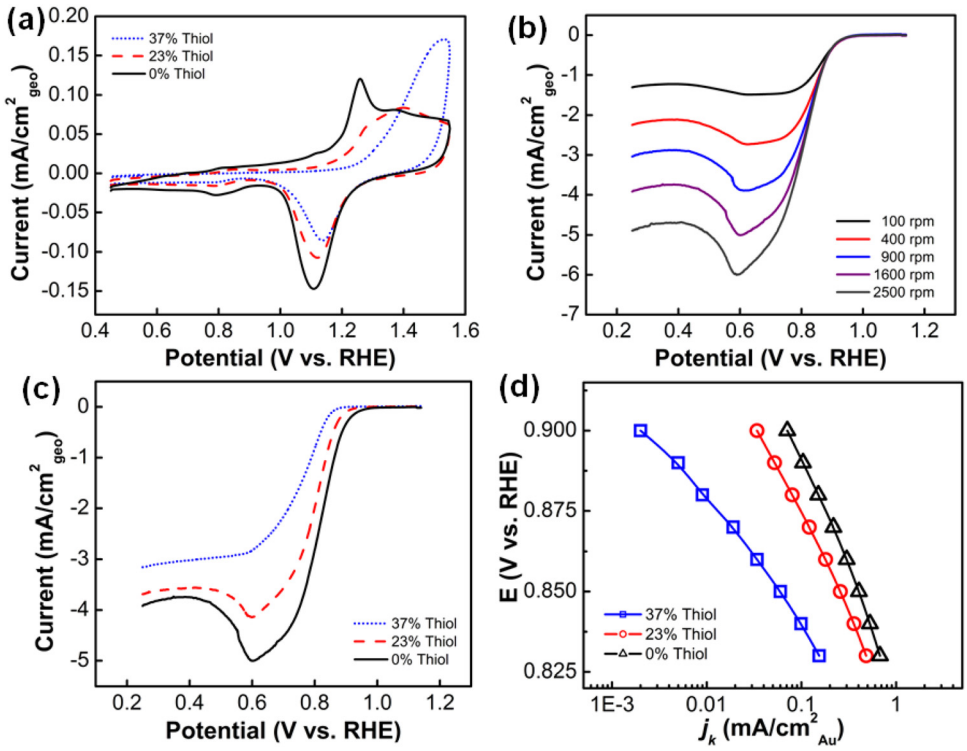

Figure 4. (Color online) (a) Cyclic voltammogram of pristine polycrystalline Au and hexanethiol (C_6S) modified Au disk in Ar-saturated 0.1 M KOH at a scan rate of 20 mV/s. (b) ORR polarization curves of pristine Au RDE in O_2-saturated 0.1 M KOH at different rotation rates and a scan rate of 10 mV/s. (c) O_2 polarization curve of pristine and C_6S-modified Au RDEs in O_2 saturated 0.1 M KOH at 1600 rpm and as can rate of 10 mV/s. (d) Tafel plots of ORR specific activity of pristine and C_6S-modified Au collected at 1600 rpm as a function of potential. All the currents in Figs. 4a–4c were normalized by the geometry area of Au disk.

nm (Fig. 3c) were higher (by ~1.5 times) than those of Au NPs of 3 nm reported previously,[12] which can be attributed to less surfactant coverage on Au NPs synthesized in the method reported herein.

Using the Koutecky-Levich equation and the electrochemically active surface area of Au, the intrinsic ORR activity (mA/cm$^2_{Au}$) of Au NPs/MWNTs of 3.4 nm was obtained as a function of potential (Fig. 3d). The intrinsic ORR activity of Au NPs of 3.4 nm (0.09 mA/cm$^2_{Au}$ at 0.85 V vs. RHE) is considerably lower than that of single-crystal Au surfaces such as (001) (10 mA/cm$^2_{Au}$) (Ref. 14) and (111) (0.3 mA/cm$^2_{Au}$).[17] While Au NPs of 3.4 nm prepared in this study have lower intrinsic ORR activity than Au cubes of 41 nm (Ref. 13) (1.1 mA/cm^2 at 0.85 V vs. RHE) reported previously, they are more active than that of spherical Au NPs with comparable NP morphologies (0.04 mA/cm^2).[26] It is interesting to note that the intrinsic ORR activity of Au NPs/MWNTs of 3.4 nm (3.5mA/cm^2 at 0.53 V vs. RHE in Fig. 3d) is considerably higher than that of Au NPs of 3 nm (3.5 mA/cm^2 at 0.41 V vs. RHE),[10] which ORR activity might be reduced by polymer blocking of surface Au atoms.

In order to further examine the thiol influence on the intrinsic ORR activity of Au, we employed a polycrystalline Au disk modified with different C_6S coverage. Figure 4a shows CVs of pristine and C_6S-modified Au RDEs in Ar-saturated 0.1 M KOH. The ESA of Au disk determined from the CVs was 0.75, 0.58 and 0.47 cm$^2_{Au}$, corresponding 0% (pristine Au), 23% and 37% C_6S coverage on the Au surface, respectively. Figure 4c compares background-corrected ORR polarization curves of pristine Au RDE and 23 and 37% C_6S-covered Au at 1600 rpm, from which the intrinsic ORR activity (i_k) as a function of potential were extracted from the Koutecky-Levich analysis[16] (Fig. 4d). Interestingly, the intrinsic ORR activity was found to decrease considerably with increasing C_6S coverage on Au, indicating thiol functional groups not only block ESA but also reduce intrinsic ORR activity of surface atoms. In addition, the diffusion-limiting current was shown to decrease with increasing C_6S coverage, from which the number of electron transfer in ORR was found to decrease from 4-electron reduction for pristine Au to 2-electron reduction for 37% C_6S-covered Au. Therefore, the strong influence of the coverage of C_6S on the ORR activity and mechanism of polycrystalline Au supports that the enhanced ORR activity of Au NPs/MWNTs with increasing annealing temperature can be attributed to the removal of thiols from the surfaces of Au NPs.

Conclusions

In this study, we have demonstrated the self-assembly of Au atoms onto thiol-functionalized MWNTs and the formation of Au NPs on the MWNTs in the range from 1.9 ± 0.4 to 3.4 ± 0.5 nm by controlling the annealing temperature. 3.4 nm Au NPs/MWNTs showed higher intrinsic and mass ORR activity than that of atomic Au and 1.9 nm Au NPs/MWNTs, which can be attributed to removal of thiols on the Au NP surfaces with increasing annealing temperature. This hypothesis is supported by additional ORR measurements of C_6S modified disks, which showed that the intrinsic ORR activity of electrochemically active Au was reduced greatly by the C_6S coverage on the surface. The understanding has led to the development of spherical Au NPs less than 5 nm with the highest ORR activity reported to date. These results emphasize that understanding the effect of surfactants is very important for enhancing catalytic activity as well as for tuning particle sizes of very small metal NPs.

Acknowledgments

This work was supported by the MRSEC Program of the National Science Foundation under the award number DMR – 0819762 and the U.S Department of Energy (DE-AC02-98CH10886) through Brookhaven National Laboratory. S.W.L. acknowledges a Samsung scholarship from the Samsung Foundation of Culture. The authors thank Ethan Crumlin for collecting XPS data.

References

1. R. Sardar, A. M. Funston, P. Mulvaney, and R. W. Murray, *Langmuir*, **25**, 13840 (2009).
2. O. Varnavski, G. Ramakrishna, J. Kim, D. Lee, and T. Goodson, *J. Am. Chem. Soc.*, **132**, 16 (2010).
3. B. E. Hayden, D. Pletcher, and J. P. Suchsland, *Angew. Chem.-Int. Ed.*, **46**, 3530 (2007).
4. P. Diao, D. F. Zhang, M. Guo, and Q. Zhang, J. Catal., **250**, 247 (2007).
5. B. Guo, S. Z. Zhao, G. Y. Han, and L. W. Zhang, *Electrochim. Acta*, **53**, 5174 (2008).

6. J. Kim, S. W. Lee, P. T. Hammond, and Y. Shao-Horn, *Chem. Mater.*, **21**, 2993 (2009).
7. M. S. El-Deab and T. Ohsaka, *Electrochim. Acta*, **47**, 4255 (2002).
8. C. Jeyabharathi, S. S. Kumar, Gobichettipalayam, V. M. Kiruthika, and K. L. N. Phani, *Angew. Chem.-Int. Ed.*, **49**, 2925 (2010).
9. W. S. Baker, J. J. Pietron, M. E. Teliska, P. J. Bouwman, D. E. Ramaker, and K. E. Swider-Lyons, *J. Electrochem. Soc.*, **153**, A1702 (2006).
10. W. Tang, H. F. Lin, A. Kleiman-Shwarsctein, G. D. Stucky, and E. W. McFarland, *J. Phys. Chem. C*, **112**, 10515 (2008).
11. M. J. Hostetler, J. E. Wingate, C. J. Zhong, J. E. Harris, R. W. Vachet, M. R. Clark, J. D. Londono, S. J. Green, J. J. Stokes, G. D. Wignall, et al., *Langmuir*, **14**, 17 (1998).
12. Y. Lee, A. Loew, and S. H. Sun, *Chem. Mater.*, **22**, 755.
13. J. Hernandez, J. Solla-Gullon, E. Herrero, A. Aldaz, and J. M. Feliu, *J. Phys. Chem. C*, **111**, 14078 (2007).
14. B. B. Blizanac, C. A Lucas, M. E. Gallagher, M. Arenz, P. N. Ross, and N. M. Markovic, *J. Phys. Chem. B*, **108**, 625 (2004).
15. J. Liu, A. G. Rinzler, H. J. Dai, J. H. Hafner, R. K. Bradley, P. J. Boul, A. Lu, T. Iverson, K. Shelimov, C. B. Huffman, et al., *Science*, **280**, 1253 (1998).
16. H. Angersteinkozlowska, B. E. Conway, A. Hamelin, and L. Stoicoviciu, *J. Electroanal. Chem.*, **228**, 429 (1987).
17. F. H. B. Lima, J. Zhang, M. H. Shao, K. Sasaki, M. B. Vukmirovic, E. A. Ticianelli, and R. R. Adzic, *J. Phys. Chem. C*, **111**, 404 (2007).
18. A. J. Bard and L. R. Faulkner, *Electrochemical Methods Fundamentals and Applications*, p. 226, John Wiley & Sons, New York (2001).
19. Z. Y. Huo, C. K. Tsung, W. Y. Huang, X. F. Zhang, and P. D. Yang, *Nano Lett.*, **8**, 2041 (2008).
20. Y. T. Kim, K. Ohshima, K. Higashimine, T. Uruga, M. Takata, H. Suematsu, and T. Mitani, *Angew. Chem.-Int. Ed.*, **45**, 407 (2006).
21. F. G. Shi, *J. Mater. Res.*, **9**, 1307 (1994).
22. L. Liu, T. X. Wang, J. X. Li, Z. X. Guo, L. M. Dai, D. Q. Zhang, and D. B. Zhu, *Chem. Phys. Lett.*, **367**, 747 (2003).
23. L. Q. Jiang and L. Gao, *Carbon*, **41**, 2923 (2003).
24. G. TremiliosiFilho, L. H. DallAntonia, and G. Jerkiewicz, *J. Electroanal. Chem.*, **422**, 149 (1997).
25. S. Strbac and R. R. Adzic, *J. Electroanal. Chem.*, **403**, 169 (1996).
26. J. Hernandez, J. Solla-Gullon, E. Herrero, J. M. Feliu, and A. Aldaz, *J. Nanosci. Nanotechnol.*, **9**, 2256 (2009).